OPEN ACCESS Freely available online

PLOS ONE

Site-Specific Perturbations of Alpha-Synuclein Fibril Structure by the Parkinson's Disease Associated Mutations A53T and E46K

Luisel R. Lemkau[1], Gemma Comellas[2], Shin W. Lee[1], Lars K. Rikardsen[1], Wendy S. Woods[3], Julia M. George[3], Chad M. Rienstra[1,2,4]*

1 Department of Chemistry, University of Illinois at Urbana-Champaign, Urbana, Illinois, United States of America, **2** Center for Biophysics and Computational Biology, University of Illinois at Urbana-Champaign, Urbana, Illinois, United States of America, **3** Department of Cell and Developmental Biology, University of Illinois at Urbana-Champaign, Urbana, Illinois, United States of America, **4** Department of Biochemistry, University of Illinois at Urbana-Champaign, Urbana, Illinois, United States of America

Abstract

Parkinson's disease (PD) is pathologically characterized by the presence of Lewy bodies (LBs) in dopaminergic neurons of the substantia nigra. These intracellular inclusions are largely composed of misfolded α-synuclein (AS), a neuronal protein that is abundant in the vertebrate brain. Point mutations in AS are associated with rare, early-onset forms of PD, although aggregation of the wild-type (WT) protein is observed in the more common sporadic forms of the disease. Here, we employed multidimensional solid-state NMR experiments to assess A53T and E46K mutant fibrils, in comparison to our recent description of WT AS fibrils. We made *de novo* chemical shift assignments for the mutants, and used these chemical shifts to empirically determine secondary structures. We observe significant perturbations in secondary structure throughout the fibril core for the E46K fibril, while the A53T fibril exhibits more localized perturbations near the mutation site. Overall, these results demonstrate that the secondary structure of A53T has some small differences from the WT and the secondary structure of E46K has significant differences, which may alter the overall structural arrangement of the fibrils.

Citation: Lemkau LR, Comellas G, Lee SW, Rikardsen LK, Woods WS, et al. (2013) Site-Specific Perturbations of Alpha-Synuclein Fibril Structure by the Parkinson's Disease Associated Mutations A53T and E46K. PLoS ONE 8(3): e49750. doi:10.1371/journal.pone.0049750

Editor: Elisa Greggio, University of Padova, Italy

Received April 30, 2012; **Accepted** October 17, 2012; **Published** March 7, 2013

Funding: National Institutes of Health R01-GM073770; National Institutes of Health S10RR025037-01; Novartis Predoctoral Fellowship to LRL; Caja Madrid Fellowship to GC. The funders had no role in study design, data collection and analysis, decision to publish, or preparation of the manuscript.

Competing Interests: The authors have declared that no competing interest exists.

* E-mail: rienstra@illinois.edu

Introduction

Aggregation of the neuronal protein alpha-synuclein (AS) is strongly implicated in both sporadic and familial forms of Parkinson's disease (PD), and with a variety of other neurodegenerative diseases collectively termed synucleinopathies. AS is the main protein component of Lewy bodies, intraneuronal cytoplasmic inclusions that are the defining neuropathological hallmark of PD [1]. Missense mutations in AS, including A53T [2], A30P [3], and E46K [4], are associated with early-onset disease, suggesting that the mutant proteins differ either in their aggregation propensity or in the stability or toxicity of the resultant aggregated species.

Like wild-type (WT) AS, the mutant proteins A30P, E46K and A53T are largely unstructured in solution [5,6,7]. However, the mutant proteins differ in their fibrillation kinetics *in vitro*; A53T and E46K fibrillize more rapidly than WT [7,8], while A30P fibrillizes more slowly, preferentially adopting a protofibrillar intermediate state [9]. To better resolve the potential similarities and differences among fibrils comprised of mutant and WT AS, we have employed magic angle spinning (MAS) solid-state nuclear magnetic resonance (SSNMR) spectroscopy. This technique is uniquely suited to structural studies of amyloid proteins, such as fibrillar AS [10,11,12,13], which are insoluble and do not form X-ray diffraction-quality crystals. Several SSNMR-derived structures or structural models of amyloid fibrils now have been deposited in the protein data bank (PDB) [14,15,16,17,18]. Recently, we used MAS SSNMR to demonstrate that the A30P mutation does not affect the secondary structure of AS fibrils when compared site-specifically with WT AS fibrils [19].

The current study focuses on the A53T and E46K mutant fibrils. While previous reports indicated significant structural differences between WT and A53T fibrils [20], those studies were complicated by batch-to-batch variability in fibril polymorphs for the WT protein [10]. We have established carefully controlled sample preparation conditions that allow reproducible measurements of AS chemical shifts [21] and have subsequently made extensive assignments of the fibril core of WT protein [12]. The same protocol for fibril preparation that we used for WT protein is also applicable to the mutant proteins [19], allowing a more direct and complete comparison of WT and mutant fibrils. Here we show that, in contrast to a prior report [10], A53T fibrils have a highly similar secondary structure to WT fibrils, with small, localized perturbations near the mutation site, as well as for some residues numbered in the range 60–70 and 80–90. E46K fibrils present larger perturbations in secondary structure, which we attribute to the large electrostatic alteration at position 46.

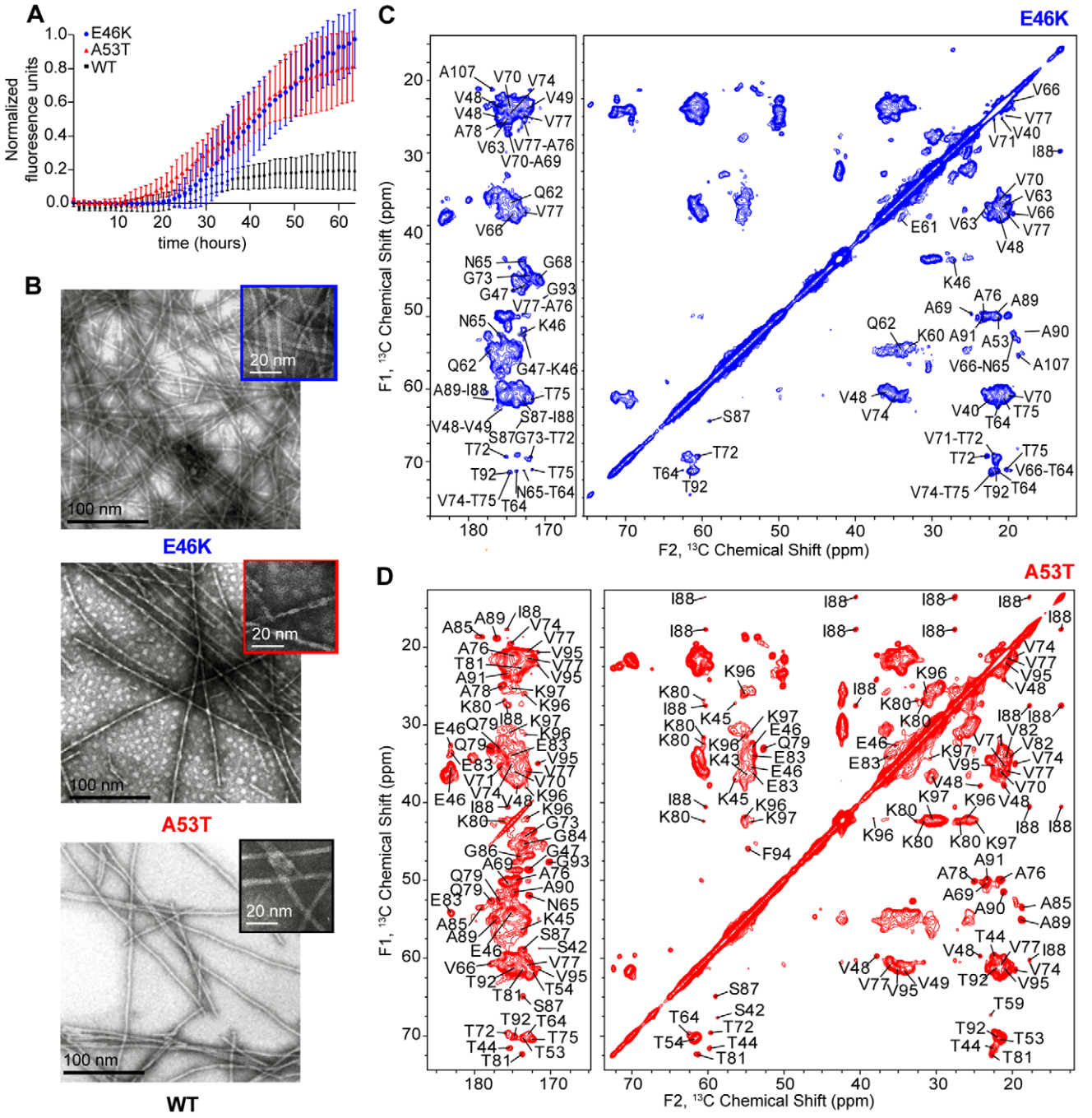

Figure 1. Fibrils of mutant AS proteins prepared *in vitro* have a highly homogeneity and morphology similar to WT fibrils. (A) AS fibrils formation of (blue circles) E46K, (red triangles) A53T and (black squares) WT monitored by the Thioflavin T fluorescence assay. Error bars were determined from seven replicates for each. Measurements were normalized to the highest fluorescence intensity obtained across all samples. (B) Comparison of the electron micrographs of (top) E46K, (middle) A53T and (bottom) WT AS fibrils. ^{13}C-^{13}C 2D with 50 ms DARR mixing of (C) E46K and (D) A53T AS fibrils.
doi:10.1371/journal.pone.0049750.g001

Materials and Methods

Protein sample preparation

Uniformly (U)-^{15}N, ^{13}C labeled WT, A53T and E46K AS were prepared following previously published protocols [21]. In summary, recombinant protein expression was performed in *E. coli* BL21(DE3) using minimal media supplemented with BioExpress (Cambridge Isotopes). Purification was performed by chemical lysis and two chromatographic steps (hydrophobic interaction and gel exclusion), resulting in ~60 mg of pure protein from each L of culture. Sample purity was confirmed by SDS-PAGE gel electrophoresis and mass spectrometry.

α-Synuclein fibrillation

Solutions of monomeric (WT, A53T or E46K) full-length AS (1 mM, 50 mM phosphate buffer, pH 7.5, 0.02% azide, 0.1 mM

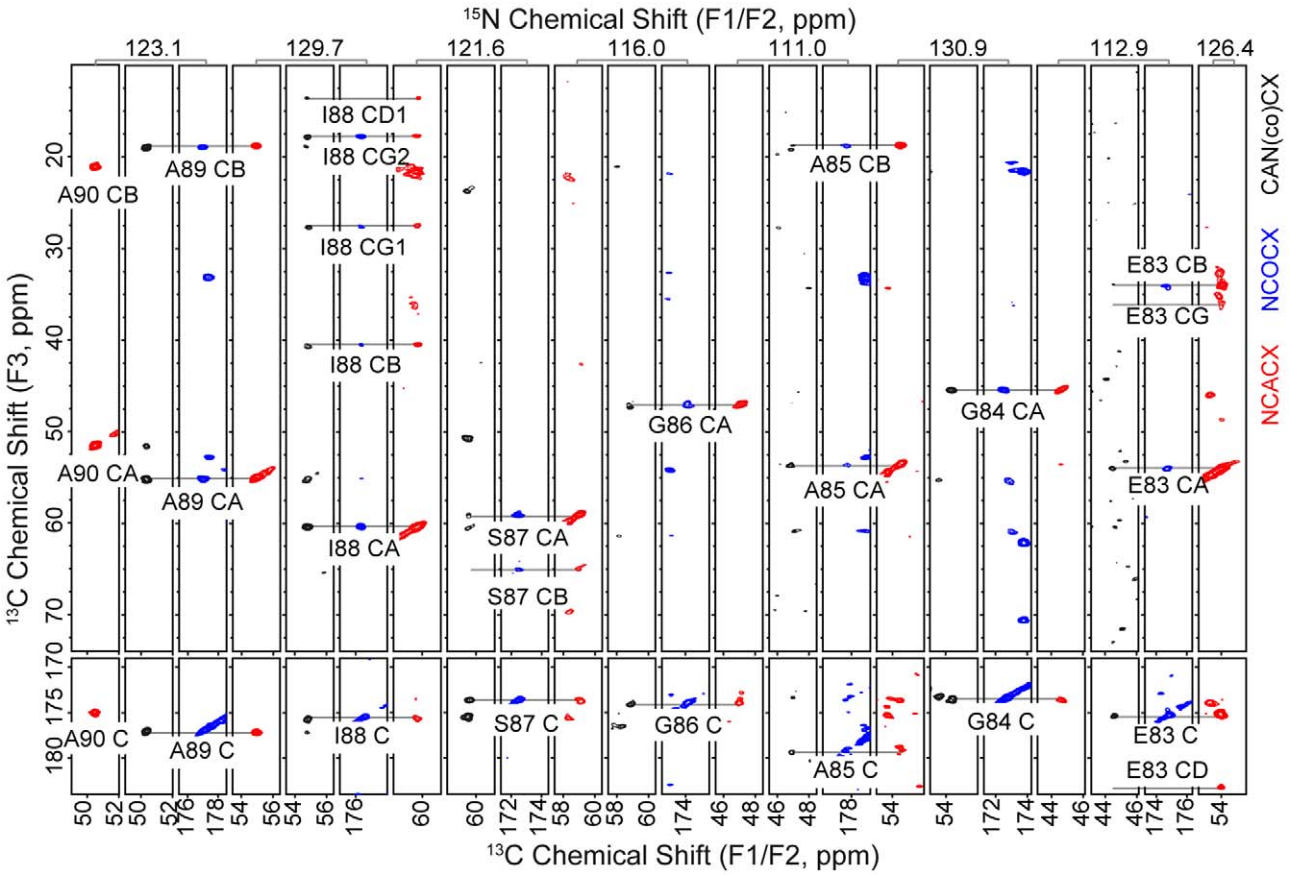

Figure 2. Sequential backbone-walk used to obtain the chemical shift assignments of A53T. Illustration of backbone connectivity through the NCACX (red), NCOCX (blue) and CAN(co)CX (black) spectra of residues A90-E83. In all cases the homonuclear mixing was achieved with 50 ms DARR.
doi:10.1371/journal.pone.0049750.g002

EDTA) were syringe filtered (0.22 μm) and seeded with natural abundance AS fibrils of the corresponding protein (WT, A53T or E46K). Samples were then incubated with shaking (200 rpm) at 37°C, as previously described [21].

Electron microscopy

A53T, E46K and WT AS fibril samples were treated with Karnovsky's fixative. After negatively staining with 2% ammonium molybdate (w/v), samples were applied on formvar carbon coated grids (300 mesh). Samples were viewed with a Hitachi H600 Transmission Electron Microscope operating at 75 kV.

α-Synuclein fibril preparation for solid-state NMR experiments

After 3 weeks of fibrillation, samples were ultracentrifuged for 1 hr at 100,000 *g*. The resultant pellets were washed with distilled water and ultracentrifuged again for 1 hr at 100,000 *g*. The supernatant was removed and the fibril pellets were dried under a stream of N_2 (*g*) until the final mass was unchanged. The dry powders were packed into 3.2 mm (thin or standard wall) NMR rotors (Varian, Inc., Palo Alto and Walnut Creek, CA and Fort Collins, CO; now part of Agilent Technologies, Santa Clara, CA and Loveland, CO), rehydrated to 36% water by mass and kept hydrated by Kel-F and rubber spacers, as previously described [12].

Solid-state NMR data collection and analysis

A 14.1 Tesla (600 MHz, ^{1}H frequency) Agilent Infinity Plus spectrometer equipped with a 3.2 mm T3 Agilent Balun^{TM} ^{1}H-^{13}C-^{15}N MAS probe, was utilized to perform all E46K SSNMR experiments. A 17.6 Tesla (750 MHz, ^{1}H frequency) Agilent VNMRS spectrometer equipped with a Varian 3.2 mm Balun^{TM} ^{1}H-^{13}C-^{15}N MAS probe, was utilized to perform all A53T SSNMR experiments. Experiments utilized tangent ramped cross polarization [22] and SPINAL-64 [23,24] ^{1}H decoupling during acquisition and evolution periods with ~75 kHz of field strength. For 3D ^{15}N-^{13}C-^{13}C and ^{13}C-^{15}N-^{13}C correlation experiments, band-selective SPECIFIC cross-polarization (CP) [25] was employed for heteronuclear polarization transfer between ^{15}N and ^{13}C and DARR [26] mixing for ^{13}C homonuclear polarization transfer. All E46K experiments were acquired under 13.3 kHz MAS and at a variable temperature (VT) of 10°C. All A53T experiments were acquired under 12.5 kHz MAS and at a VT temperature of 0°C. 1D ^{13}C and 2D ^{13}C-^{13}C were also collected at a range of temperatures from −10°C to +20°C to confirm that the spectra did not depend to a significant extent on the exact sample temperature. Chemical shifts were externally referenced using adamantane, with the downfield ^{13}C peak at 40.48 ppm [27].

NMR datasets were processed in NMRPipe [28] by applying back linear prediction to the direct dimension, and in all dimensions Lorentzian-to-Gaussian apodization was applied prior to zero filling and Fourier transformation. Peak picking, assign-

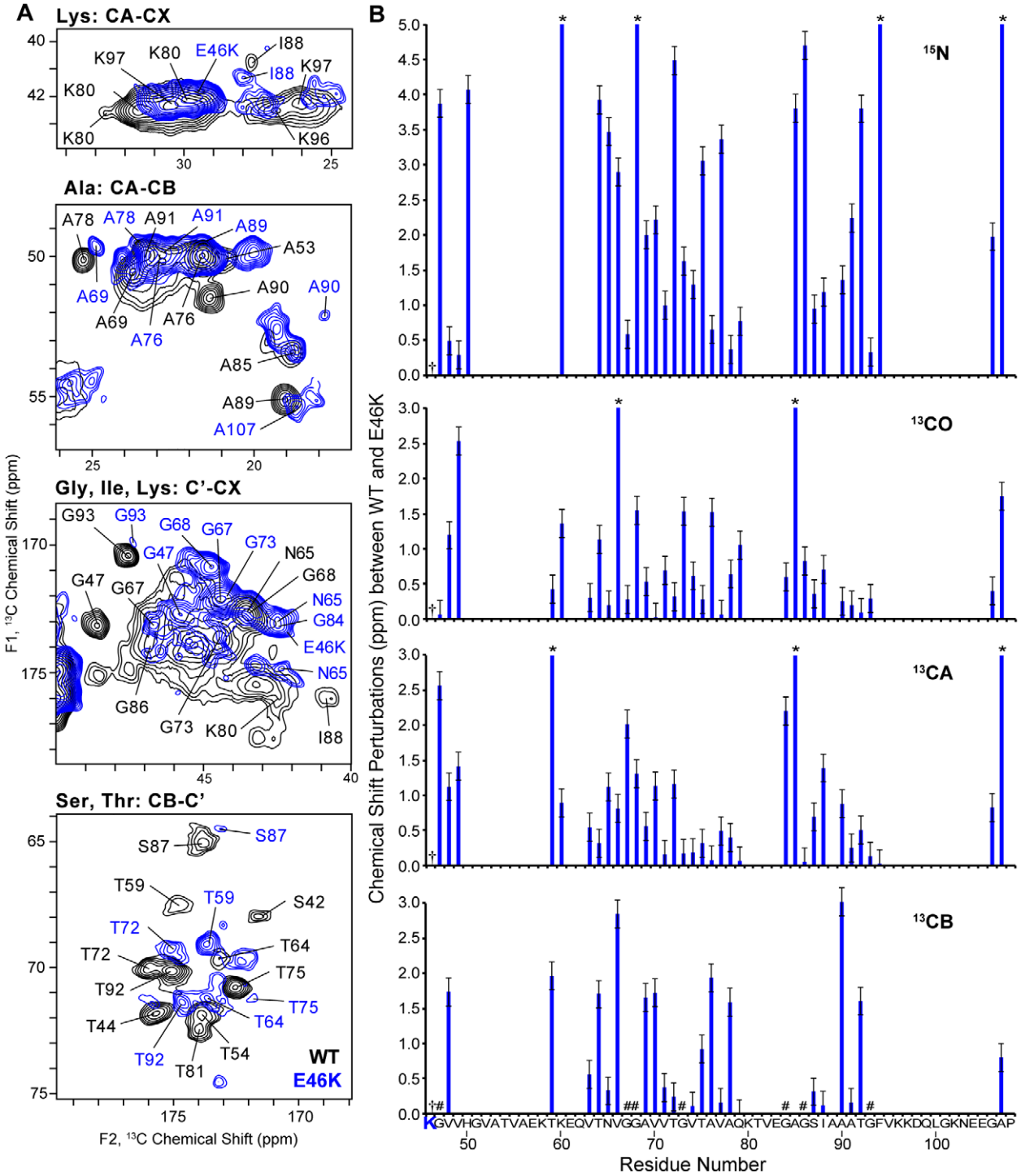

Figure 3. The E46K mutation causes major chemical shift perturbations throughout the AS fibril sequence. (A) Expansions of ^{13}C-^{13}C 2D spectral overlays (50 ms DARR mixing) of WT (black) and E46K (blue) AS fibril samples. (B) Plot of chemical shift perturbations between WT and E46K chemical shifts versus residue number. Residues labeled as (*) correspond to perturbations greater than 5 ppm (^{15}N) or 3 ppm (^{13}C). Residues labeled as (#) correspond to glycines. The mutation is indicated with (†). Error bars correspond to the chemical shift variations from one WT batch to another. WT chemical shift assignments were obtained from the BMRB #16939.
doi:10.1371/journal.pone.0049750.g003

ments and peak heights were obtained with NMRViewJ software [29] using Gaussian peak integration methods. Chemical shifts were deposited in the Biological Magnetic Resonance Bank (BMRB codes #18208 and #18207 for E46K and A53T, respectively).

Results and Discussion

Sample characterization

Monomers of each AS sample were incubated at 37°C and 200 rpm shaking, and fibrillation kinetics were measured by ThT

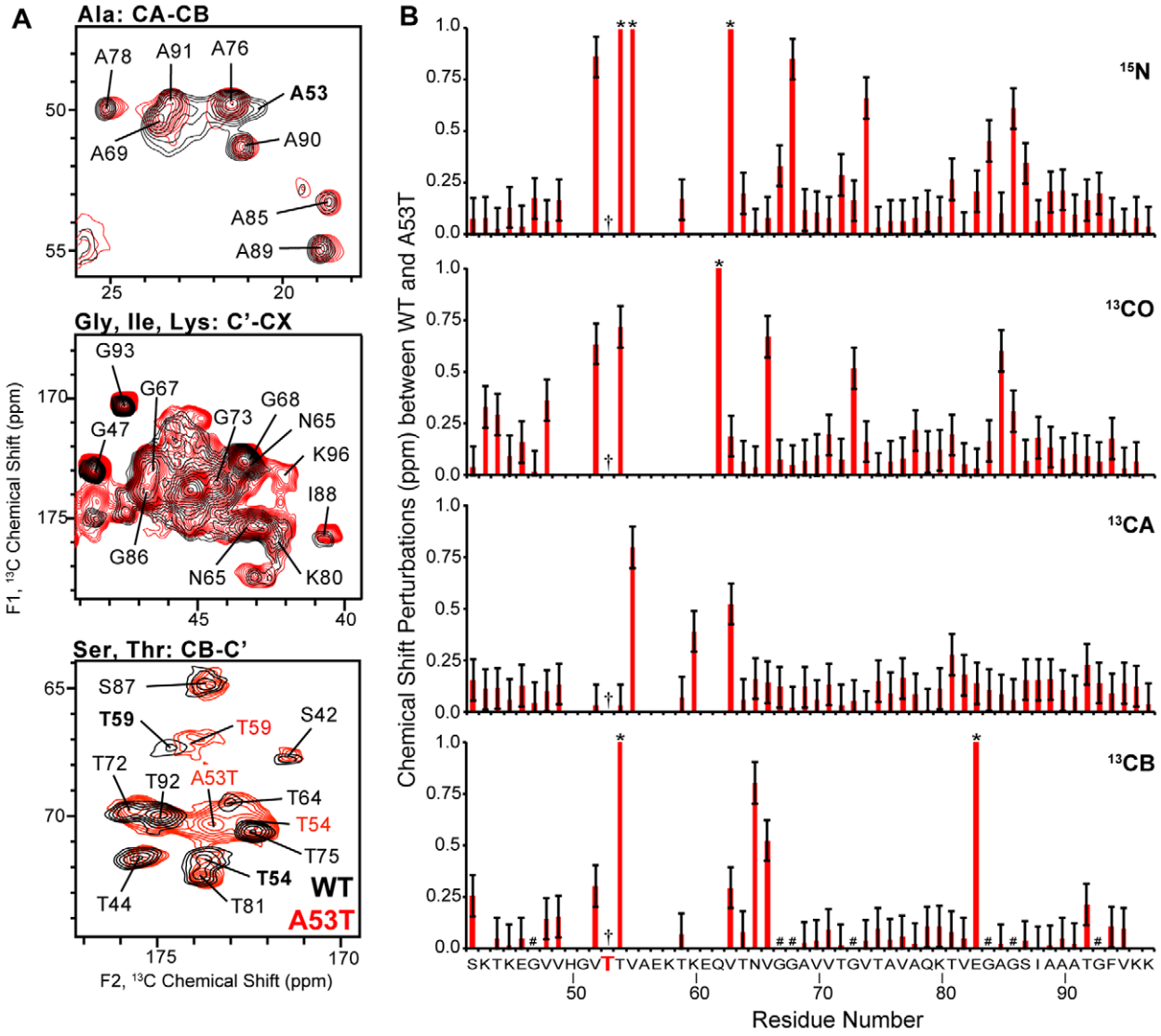

Figure 4. The A53T mutation causes minor perturbations throughout the AS fibril sequence. (A) Expansions of ^{13}C-^{13}C 2D spectral overlays (50 ms DARR mixing, 600 MHz ^{1}H frequency and 13.3 kHz MAS) of WT (black) and A53T (red) AS fibril samples. (B) Plot of the chemical shift perturbations between WT and A53T chemical shifts versus residue number. Residues labeled as (*) correspond to perturbations above 1 ppm. Residues labeled as (#) correspond to glycines. The mutation is indicated with (†). Error bars correspond to the chemical shift variations from one WT batch to another. WT chemical shift assignments were obtained from the BMRB #16939.
doi:10.1371/journal.pone.0049750.g004

fluorescence under identical conditions to the preparation of the NMR samples. The A53T and E46K mutant proteins exhibited accelerated fibrillation kinetics relative to WT (Figure 1A), consistent with previous reports [7,8,9,30,31,32,33]. Previous studies indicate possible differences in morphology between the mutants and WT based on FE and AFM investigations [13,34], while similar morphologies were observed by electron microscopy [32,35] (Figure 1B). Under these conditions, the rehydrated SSNMR samples of both mutants yielded high resolution ^{13}C-^{13}C 2D spectra (Figure 1C,D), with narrow linewidths (<0.2 ppm) indicating a high degree of homogeneity throughout the fibrils, as previously observed for the WT [12]. The spectra were therefore determined to have more than sufficient sensitivity and resolution to perform chemical shift assignments in combination with 3D experiments.

Chemical shift comparison of the A53T and E46K mutants versus wild-type

Chemical shifts were assigned using the standard complement of multidimensional SSNMR experiments for both mutant fibrils, as listed in Table S1. The analysis proceeded by *de novo* backbone walks and did not rely upon the WT assignments. Common amide frequencies in the three 3D spectra—NCACX, NCOCX and CAN(co)CX—were used to establish sequential connectivities, and side-chain chemical shifts were confirmed in combination with the 2D ^{13}C-^{13}C spectra, resulting in site-specific assignments, as illustrated in Figure 2. Assignments were further confirmed by examining the strips through the CA frequencies in the NCACX and CAN(co)CX experiments and the carbonyl carbon (CO) frequency in the NCOCX and CAN(co)CX experiments. The residues assigned sequentially for E46K were K46-V49, T59-Q79, G84-F94 and G106-P108. The residues assigned sequentially for

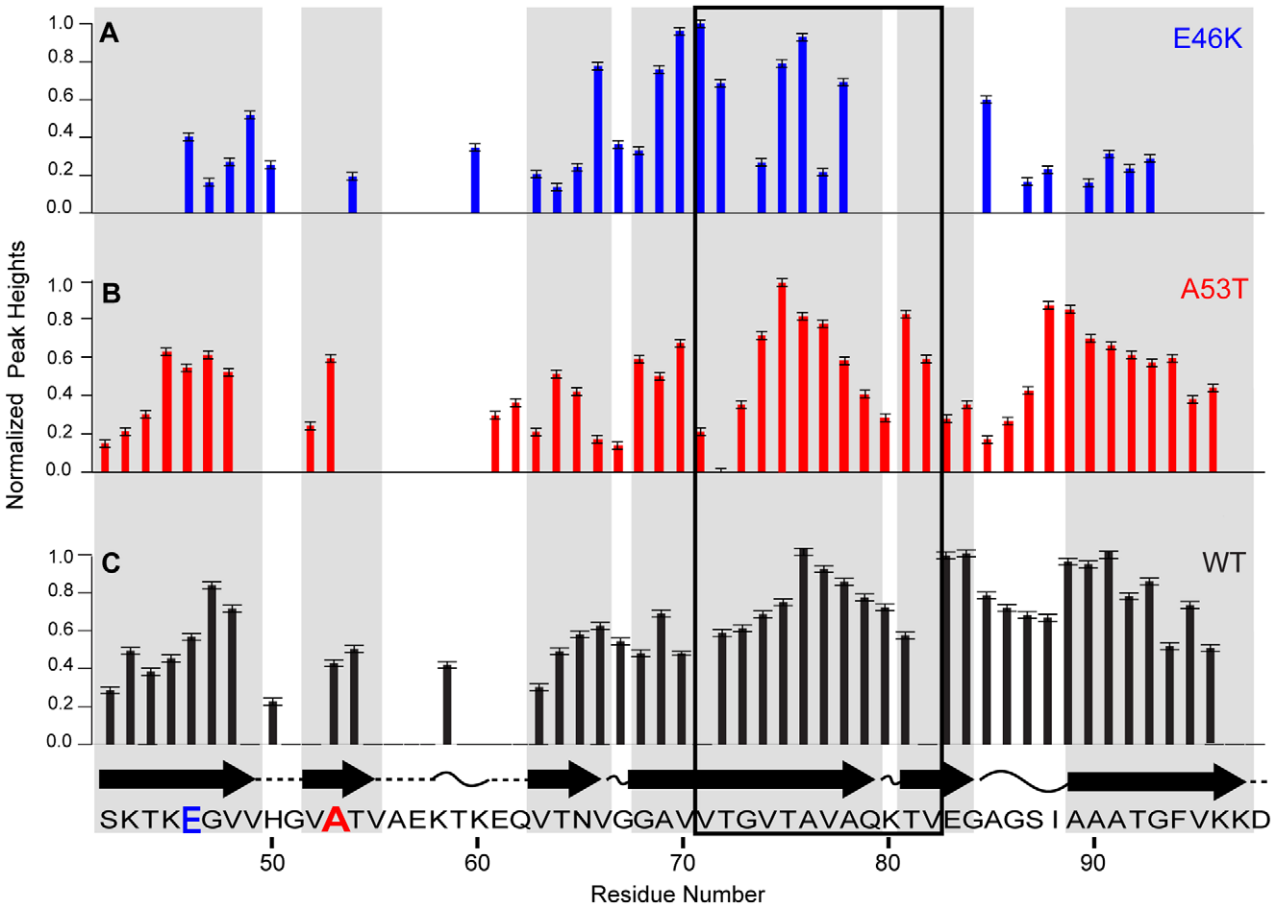

Figure 5. Comparison of relative signal intensities between the WT, E46K and A53T. Normalized peak heights from CANCO experiments as a function of residue number for (A) E46K, (B) A53T and (C) WT. Error bars correspond to the noise level. Representation of the secondary structure of WT AS fibrils based on TALOS+ analysis (β-strands, arrows; turn or loop curved lines; not predicted, dashed lines) from Comellas *et al*. Regions described to be essential for the fibril formation by Giasson *et al* are highlighted with a black outlined box. Grey boxes highlight the located of the WT β-strands.
doi:10.1371/journal.pone.0049750.g005

A53T were S42-V49, V52-V55 and T59-K97. Chemical shift assignments are included in Tables S2 and S3 for E46K and A53T, respectively.

Chemical shifts (especially for ^{13}C) depend strongly upon secondary structure [36,37,38,39,40] and therefore serve as highly reliable tool for evaluating structural perturbations arising from the AS mutations. As shown in Figure 3, E46K exhibits chemical shift perturbations throughout the amino acid sequence. In the WT secondary structure [12], residue E46 is located in one of the long β-sheet strands. Therefore, it is not surprising that E46K mutation, where an ionic residue is replaced with a cationic residue at pH 7.4, leads to major chemical shift perturbations ($|\Delta\delta|_{avg}$~1.6 ppm) versus the WT throughout the fibril core, due to the alternation in electrostatics. In contrast, the A53T mutant exhibits relatively minor chemical shift perturbations ($|\Delta\delta|_{avg}$~0.5 ppm), and the perturbations are very much localized located in certain regions of the fibril core. The ^{13}CA and ^{15}N chemical shift perturbations (Figure 4) in A53T AS fibrils versus the WT are found near the mutation site, as well as in the 60 s and 80 s.

Relative signal intensities and secondary structure comparison between the mutants and wild-type

The relative rigidity of regions within the fibril core was evaluated based on the signal intensities of a dipolar-based 3D CANCO experiment. Our recent investigations demonstrated that the region reported by Giasson *et al* to be responsible for fibrillation (residues 71–82 for the WT [41]) exhibited some of the highest signal intensities within the fibril core [12]. Together with several other site-specific measurements, we demonstrated that these residues are among the most rigid residues in the structure. As demonstrated in Figure 5, these regions are within the stronger regions of the core compared to the other signals in both mutants. The site-specific pattern of residues 71–82 and the relative signal intensity in the 90 s versus other regions in the sequence is somewhat different for E46K versus WT or A53T.

Because chemical shifts are highly sensitive to atomic environment [36,37,38,39,40], backbone dihedral angles (Φ and Ψ) and secondary structure can be predicted in a semi-empirical manner using the TALOS+ program [42] to obtain the backbone dihedral angles and secondary structure for E46K and A53T AS fibrils (Figure 6). While the TALOS+ results demonstrate that A53T exhibits small changes in secondary structure compared to the WT, E46K exhibits substantial chemical shift changes relative to WT, indicating differences in secondary structure patterns. These

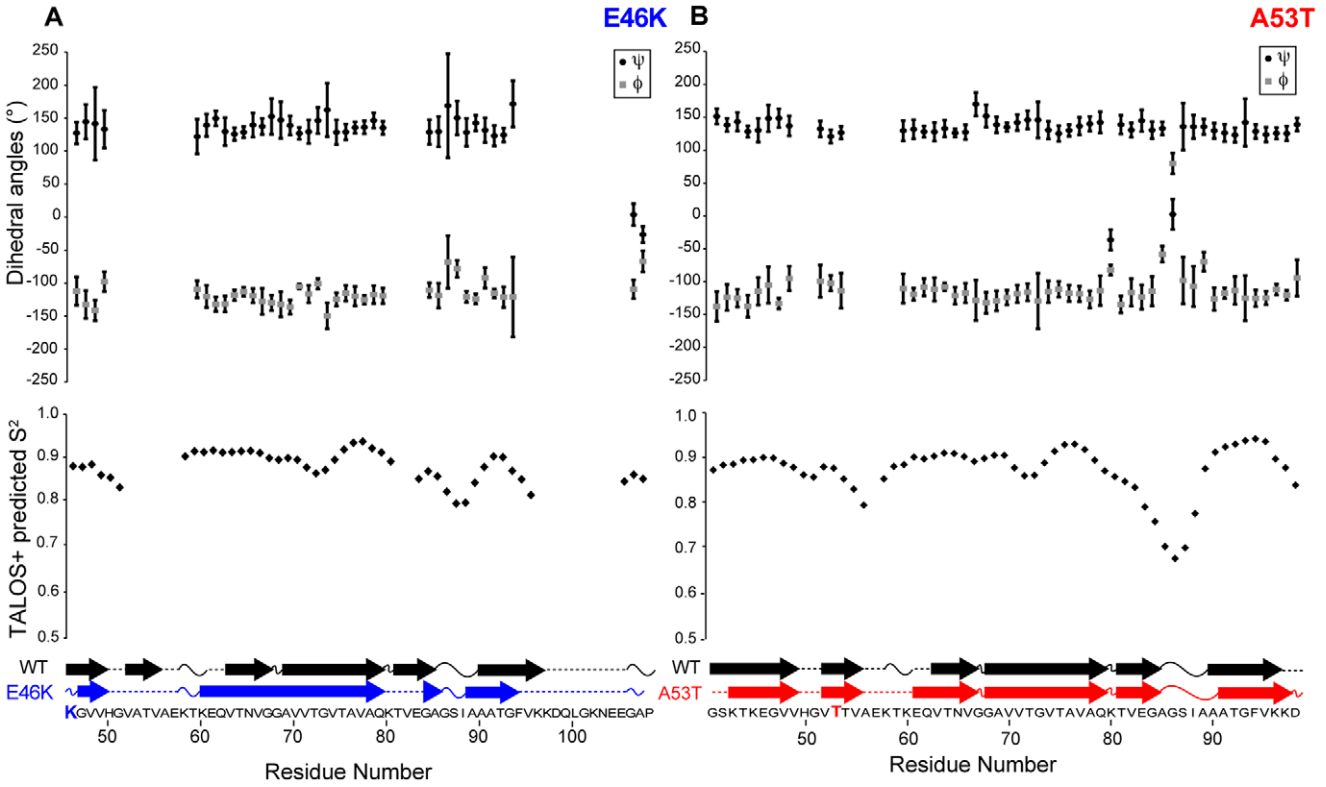

Figure 6. TALOS+ predicted backbone dihedral angles ψ and ϕ as a function of residue number. (A) E46K and (B) A53T AS fibrils. Error bars based on the 10 best TALOS+ database matches. Representation of the secondary structure for WT (black), E46K (blue) and A53T (red) AS fibrils based on TALOS+ analysis (β-strands, arrows; turn or loop curved lines; not predicted, dashed lines). WT TALOS+ results based on those from Comellas *et al*.
doi:10.1371/journal.pone.0049750.g006

results demonstrate that the secondary structure is somewhat similar for A53T and WT; whether this arises from a common three-dimensional fold remains to be determined. In contrast, for E46K, the chemical shift values indicate significant differences in secondary structure for the E46K mutant relative to WT; it is likely that the overall structural arrangement of the E46K mutant therefore is different from that of the WT protein.

Conclusion

In summary, we have site-specifically compared the structures of AS fibrils from the E46K and A53T early-onset PD mutants to the WT using MAS SSNMR. Our results demonstrate minor site-specific perturbations near the mutation site, the 60 s and 80 s for A53T and large chemical shift perturbations within the entire core for E46K. In addition, they reveal that the residues described to be essential for the WT fibrils formation by Giasson *et al* are also within some of the most stable residues in the core for the mutants.

Taken all these results together, this study demonstrates the presence of site-specific perturbations in the fibril structure by the A53T and E46K mutants. We believe these results will assist future investigations to elucidate how these mutants affect the fibrillogenesis of AS compared to the WT in the presence of phospholipid vesicles [43,44]. These studies might be significantly relevant to understand the role of the early-onset PD mutants in the disease.

Supporting Information

Table S1 Description of the multidimensional experiments acquired to obtain *de novo* ^{13}C, ^{15}N chemical shift assignments.
(DOC)

Table S2 ^{13}C and ^{15}N chemical shift assignments of E46K AS fibrils.
(DOC)

Table S3 ^{13}C and ^{15}N chemical shift assignments of A53T AS fibrils.
(DOC)

Acknowledgments

Electron micrographs were collected at the Frederick Seitz Materials Research Laboratory, University of Illinois.

Author Contributions

Conceived and designed the experiments: LRL GC WSW JMG CMR. Performed the experiments: LRL GC SWL LKR WSW. Analyzed the data: LRL GCC WSW JMG CMR. Contributed reagents/materials/analysis tools: LRL GCC SWL LKR WSW. Wrote the paper: LRL GCC JMG CMR.

References

1. Spillantini MG, Schmidt ML, Lee VM, Trojanowski JQ, Jakes R, et al. (1997) Alpha-synuclein in Lewy bodies. Nature 388: 839–840.

2. Polymeropoulos MH, Lavedan C, Leroy E, Ide SE, Dehejia A, et al. (1997) Mutation in the alpha-synuclein gene identified in families with Parkinson's disease. Science 276: 2045–2047.

3. Kruger R, Kuhn W, Muller T, Woitalla D, Graeber M, et al. (1998) Ala30Pro mutation in the gene encoding alpha-synuclein in Parkinson's disease. Nat Genet 18: 106–108.
4. Zarranz JJ, Alegre J, Gomez-Esteban JC, Lezcano E, Ros R, et al. (2004) The new mutation, E46K, of alpha-synuclein causes Parkinson and Lewy body dementia. Ann Neurol 55: 164–173.
5. Eliezer D, Kutluay E, Bussell R, Browne G (2001) Conformational properties of alpha-synuclein in its free and lipid-associated states. J Mol Biol 307: 1061–1073.
6. Bussell R, Eliezer D (2001) Residual structure and dynamics in Parkinson's disease-associated mutants of alpha-synuclein. J Biol Chem 276: 45996–46003.
7. Fredenburg RA, Rospigliosi C, Meray RK, Kessler JC, Lashuel HA, et al. (2007) The impact of the E46K mutation on the properties of alpha-synuclein in its monomeric and oligomeric states. Biochemistry 46: 7107–7118.
8. Conway KA, Harper JD, Lansbury PT (1998) Accelerated in vitro fibril formation by a mutant alpha-synuclein linked to early-onset Parkinson disease. Nat Med 4: 1318–1320.
9. Narhi L, Wood SJ, Steavenson S, Jiang YJ, Wu GM, et al. (1999) Both familial Parkinson's disease mutations accelerate alpha-synuclein aggregation. J Biol Chem 274: 9843–9846.
10. Heise H, Hoyer W, Becker S, Andronesi OC, Riedel D, et al. (2005) Molecular-level secondary structure, polymorphism, and dynamics of full-length alpha-synuclein fibrils studied by solid-state NMR. Proc Natl Acad Sci USA 102: 15871–15876.
11. Loquet A, Giller K, Becker S, Lange A (2010) Supramolecular interactions probed by 13C-13C solid-state NMR spectroscopy. J Am Chem Soc 132: 15164–15166.
12. Comellas G, Lemkau LR, Nieuwkoop AJ, Kloepper KD, Ladror DT, et al. (2011) Structured regions of α-synuclein fibrils include the early-onset Parkinson's disease mutation sites. J Mol Biol 411: 881–895.
13. Celej MS, Caarls W, Demchenko AP, Jovin TM (2009) A Triple-Emission Fluorescent Probe Reveals Distinctive Amyloid Fibrillar Polymorphism of Wild-Type alpha-Synuclein and Its Familial Parkinson's Disease Mutants. Biochemistry 48: 7465–7472.
14. Jaroniec CP, MacPhee CE, Bajaj VS, McMahon MT, Dobson CM, et al. (2004) High-resolution molecular structure of a peptide in an amyloid fibril determined by magic angle spinning NMR spectroscopy. Proc Natl Acad Sci USA 101: 711–716.
15. Ferguson N, Becker J, Tidow H, Tremmel S, Sharpe TD, et al. (2006) General structural motifs of amyloid protofilaments. Proc Natl Acad Sci USA 103: 16248–16253.
16. Iwata K, Fujiwara T, Matsuki Y, Akutsu H, Takahashi S, et al. (2006) 3D structure of amyloid protofilaments of beta2-microglobulin fragment probed by solid-state NMR. Proc Natl Acad Sci USA 103: 18119–18124.
17. Wasmer C, Lange A, Van Melckebeke H, Siemer AB, Riek R, et al. (2008) Amyloid fibrils of the HET-s(218–289) prion form a beta solenoid with a triangular hydrophobic core. Science 319: 1523–1526.
18. van Melckebeke H, Wasmer C, Lange A, Ab E, Loquet A, et al. (2010) Atomic-resolution three-dimensional structure of HET-s(218–289) amyloid fibrils by solid-state NMR spectroscopy. J Am Chem Soc 132: 13765–13775.
19. Lemkau LR, Comellas G, Kloepper KD, Woods WS, George JM, et al. (2012) A30P alpha-synuclein adopts the wild-type fibrils structure, despite slower fibrillation kinetics. J Biol Chem 287: 11526–11532.
20. Heise H, Celej MS, Becker S, Riede D, Pelah A, et al. (2008) Solid-state NMR reveals structural differences between fibrils of wild-type and disease-related A53T mutant alpha-synuclein. J Mol Biol 380: 444–450.
21. Kloepper KD, Woods WS, Winter KA, George JM, Rienstra CM (2006) Preparation of alpha-synuclein fibrils for solid-state NMR: Expression, purification, and incubation of wild-type and mutant forms. Protein Expr Purif 48: 112–117.
22. Hediger S, Meier BH, Kurur ND, Bodenhausen G, Ernst RR (1994) NMR cross-polarization by adiabatic passage through the Hartmann-Hahn condition (APHH). Chem Phys Lett 223: 283–288.
23. Fung BM, Khitrin AK, Ermolaev K (2000) An improved broadband decoupling sequence for liquid crystals and solids. J Magn Reson 142: 97–101.
24. Comellas G, Lopez JJ, Nieuwkoop AJ, Lemkau LR, Rienstra CM (2011) Straightforward, effective calibration of SPINAL-64 decoupling results in the enhancement of sensitivity and resolution of biomolecular solid-state NMR. J Magn Reson 209: 131–135.
25. Baldus M, Petkova AT, Herzfeld J, Griffin RG (1998) Cross polarization in the tilted frame: assignment and spectral simplification in heteronuclear spin systems. Mol Phys 95: 1197–1207.
26. Takegoshi K, Nakamura S, Terao T (2001) C-13-H-1 dipolar-assisted rotational resonance in magic-angle spinning NMR. Chem Phys Lett 344: 631–637.
27. Morcombe CR, Zilm KW (2003) Chemical shift referencing in MAS solid state NMR. J Magn Reson 162: 479–486.
28. Delaglio F, Grzesiek S, Vuister GW, Zhu G, Pfeifer J, et al. (1995) Nmrpipe: a Multidimensional Spectral Processing System Based On Unix Pipes. J Biomol NMR 6: 277–293.
29. Johnson B (2007) NMRViewJ. 8.1.13 ed. Newark: One Moon Scientific, Inc.
30. Li J, Uversky VN, Fink AL (2001) Effect of familial Parkinson's disease point mutations A30P and A53T on the structural properties, aggregation, and fibrillation of human alpha-synuclein. Biochemistry 40: 11604–11613.
31. Hoyer WG, Cherny D, Subramaniam V, Jovin TM (2004) Rapid self-assembly of alpha-synuclein observed by in situ atomic force microscopy. J Mol Biol 340: 127–139.
32. Choi W, Zibaee S, Jakes R, Serpell LC, Davletov B, et al. (2004) Mutation E46K increases phospholipid binding and assembly into filaments of human alpha-synuclein. FEBS Lett 576: 363–368.
33. Greenbaum EA, Graves CL, Mishizen-Eberz AJ, Lupoli MA, Lynch DR, et al. (2005) The E46K mutation in alpha-synuclein increases amyloid fibril formation. J Biol Chem 280: 7800–7807.
34. van Raaij ME, Segers-Nolten IM, Subramaniam V (2006) Quantitative morphological analysis reveals ultrastructural diversity of amyloid fibrils from alpha-synuclein mutants. Biophysical Journal 91: L96–98.
35. Serpell LC, Berriman J, Jakes R, Goedert M, Crowther RA (2000) Fiber diffraction of synthetic alpha-synuclein filaments shows amyloid-like cross-beta conformation. Proc Natl Acad Sci U S A 97: 4897–4902.
36. Wishart DS, Sykes BD, Richards FM (1991) Relationship Between Nuclear-Magnetic-Resonance Chemical-Shift and Protein Secondary Structure. J Mol Biol 222: 311–333.
37. Wishart DS, Sykes BD (1994) Chemical-Shifts as a Tool for Structure Determination. Methods in Enzymol 239: 363–392.
38. Wishart DS, Sykes BD (1994) The 13C chemical-shift index: a simple method for the identification of protein secondary structure using 13C chemical-shift data. J Biomol NMR 4: 171–180.
39. Cornilescu G, Delaglio F, Bax A (1999) Protein backbone angle restraints from searching a database for chemical shift and sequence homology. J Biomol NMR 13: 289–302.
40. Oldfield E (2002) Chemical shifts in amino acids, peptides, and protiens: From Quantum Chemistry to Drug Design. Ann Rev Phys Chem 53: 349–378.
41. Giasson BI, Murray IVJ, Trojanowski JQ, Lee VMY (2001) A hydrophobic stretch of 12 amino acid residues in the middle of alpha-synuclein is essential for filament assembly. J Biol Chem 276: 2380–2386.
42. Shen Y, Delaglio F, Cornilescu G, Bax A (2009) TALOS plus: a hybrid method for predicting protein backbone torsion angles from NMR chemical shifts. J Biomol NMR 44: 213–223.
43. Bodner CR, Maltsev AS, Dobson CM, Bax A (2010) Differential Phospholipid Binding of alpha-Synuclein Variants Implicated in Parkinson's Disease Revealed by Solution NMR Spectroscopy. Biochemistry 49: 862–871.
44. Comellas G, Lemkau LR, Zhou DH, George JM, Rienstra CM (2012) Unique structural intermediates during alpha-synuclein fibrillogenesis on phospholipid vesicles. J Am Chem Soc 134: 5090–5099.